Arab J Geosci
DOI 10.1007/s12517-015-1808-5

ORIGINAL PAPER

Evaluation of groundwater mineralization processes and seawater intrusion extension in the coastal aquifer of Oualidia, Morocco: hydrochemical and geophysical approach

Ahmed Fadili · Khalid Mehdi · Joëlle Riss · Saliha Najib · Abdelhadi Makan · Khadija Boutayab

Received: 25 August 2014 / Accepted: 20 January 2015

Abstract Oualidia city is located on the Moroccan Atlantic coast. Groundwater is the only resource for agriculture irrigation in this area. This operation is done by intensive pumping mainly in the coastal fringe. In this study, hydrochemical and geophysical methods were conducted to evaluate both composition and processes which control groundwater mineralization in Oualidia. For this purpose, 19 samples of groundwater were analyzed in major ions. The results showed that the mineralization is mainly due to sea water intrusion, especially in the first kilometer over the ocean, with abundance of Na^+ (651.3 mg/l on average) and Cl^- ions (1,425 mg/l on average). Beyond this fringe, 1 km, the mineralization is low, with an abundance of calcium (190.4 mg/l on average) and bicarbonate (241.1 mg/l on average) indicating the rock nature effect. Data interpretation from six profiles of electrical resistivity tomography (ERT), performed in the region, has led to detect seawater intrusion extension. The level assigned to the marine effect is characterized by a resistivity lower than 30 Ω m. Moreover, hydrochemical and geophysical studies were provided information on the mineralization extension in the aquifer of this zone, which is limited to 1 km from the ocean.

A. Fadili (✉) · K. Mehdi · S. Najib · K. Boutayab
Marine Géoscience and Soil Science Laboratory (URAC-45), Faculty of Science, University of Chouïb Doukkali, El Jadida, Morocco
e-mail: faahmed81@yahoo.fr

J. Riss
I2M UMR 5295 Laboratory, Environmental Civil Engineering Department, Bordeaux 1 University, Bordeaux, France

A. Makan
Water and Environment Laboratory, Faculty of Science, University of Chouïb Doukkali, El Jadida, Morocco

Published online: 05 February 2015

Keywords Groundwater mineralization · Statistical analysis · Ionic ratios · Electrical resistivity tomography

Introduction

The seawater intrusion in coastal aquifers leads to quality degradation of fresh waters. Excessive increasing groundwater exploitation lowering water tables is well known to be the primary cause of saltwater intrusion. The extent of saltwater intrusion is controlled mainly by geological characteristics of the area, hydraulic gradient, and the rate of exploitation with respect to the reload of the groundwater (Choudhury et al. 2001; Morgan and Werner 2014). Analyzing seawater intrusion in coastal aquifers requires multidisciplinary approach, combining several methods, such as geophysics and hydrochemistry. Electrical prospecting was applied by several authors to delimit the marine intrusion extension (Bugg and Lloyd 1976; Urish and Frohlich 1990; Vandam and Meulankamp 1967; Zohdy 1969; Frohlich et al. 1994; Nowroozi et al. 1999. Choudhury et al. 2001; Hodlur et al. 2010; Agoubi et al. 2013; Atwia and Masoud 2013; Hamdan and Vafidis 2013; Naidu et al. 2013; Rey et al. 2013; Sonkamble 2014). Other investigations have been focused on the processes definition and chemical reactions that characterize groundwater mineralization, and thus be responsible for the enrichment or depletion of groundwater chemical elements (Nadler et al. 1980; Tulipano and Fidelibus 1984; Fidelibus and Tulipano 1986; Pascual and Custodio 1990; Fetter 1993; Tellam 1995; Fidelibus and Tulipano 1996; Allen and Suchy 2001; Farber et al. 2004; Grassi and Cortecci 2004; Cardona et al. 2004; Banerjee et al. 2012;. Reddy 2013; Han et al. 2014; Srinivasamoorthy et al. 2014). In Morocco, several studies have applied geophysics and hydrochemistry to investigate the seawater intrusion effect on coastal aquifers salinity.

Among these studies, we cited the following: Benkabbour et al. (2004), Zouhri et al. (2008), Zouhri (2010), El Yaouti et al. (2009), Re et al. (2013), and Vinson et al. (2013).

Oualidia city, the area subject of this study, is located on the Moroccan Atlantic coast (Fig. 1), 70 km south-west of El Jadida city. The only natural water resources are those of Plioquaternaire calcareous sandstones and late Hauterivian limestones groundwater as shown in Fig. 2 (known in the region as Dridrate limestone) (Ferré 1969). In this region, groundwater exploitation is done by intensive pumping especially in the coastal fringe (Fakir et al. 2002). Intensive pumping involves fresh waters quality deterioration as a result of the seawater advancement to the inland (Fakir et al. 2002; Kaid rassou et al. 2005).

However, the aim of this study is first to identify processes and chemical reactions responsible for the salinization of Oualidia coastal aquifers and next to determine the seawater intrusion extension. For the first purpose, hydrochemical analyzes were performed on water samples issued from the wells in the area under study. For the second objective, electrical resistivity tomography (ERT) profiles were carried out in the Southern of Oualidia. Electrical models are compared with geological borehole data and hydrochemical results. The study of marine intrusion by electrical resistivity tomography is an original work in the region.

Presentation of the study area

Geographical and geological setting

Oualidia is a coastal area from the Moroccan coastal Meseta. It is marked by ridge lines of consolidated dunes formed during Quaternary transgressions and regressions (Ferré 1969). Ferré (1969) specified that the outcrops are mainly formed by consolidated dunes, sandstone and limestone, of Plioquaternaire age with 50 m thick and decreases toward the ocean. The dunes are elongated into long ridges with SW-NE orientation parallel to the shoreline (Fig. 1). Below the Plioquaternary sandstone-limestone formation, the following geological formations (Fig. 2) are found:

- Red clay layer from the late Hauterivian age which forms the wall of Plioquaternaire and the roof of the Hauterivian. Their thickness varies from 20 to 50 m with respect to the position relative to the shore. These clays disappear due to erosion near the ocean, allowing direct contact between the Plioquaternaire and Hauterivian.
- Dridrate limestone from the late Hauterivian age; 30 to 50 m thick. They constitute the second aquifer from the area.
- Blue clay from late Valanginian-Early Hauterivian. They are gray marl forming the bedrock of Dridrate limestone.
- The gypsum limestone from Jurassic, which forms the third aquifer. The presence of evaporite causes high salinity and, thus, non-exploitation of this aquifer.

Geomorphological context

To analyze the geomorphology of the study area, we have established a digital elevation model from the topographic map of the Oualidia. Modeling was performed on Arcgis software (McCoy 2004).

On the geomorphological plan, the region of Oualidia is marked on the side of the Atlantic Ocean by a low sandy

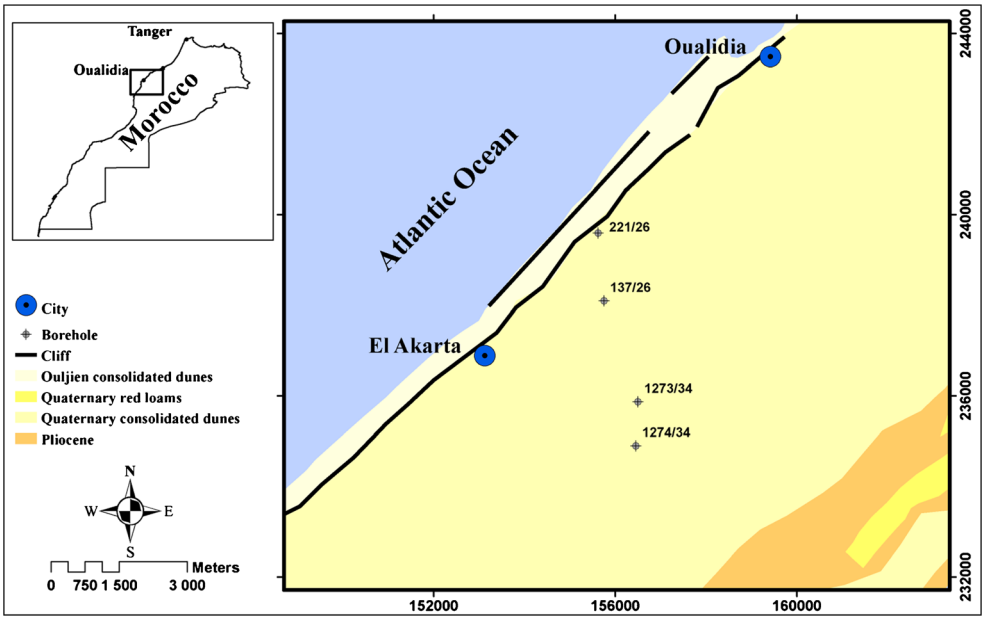

Fig. 1 Geological and geographical location of the area under study

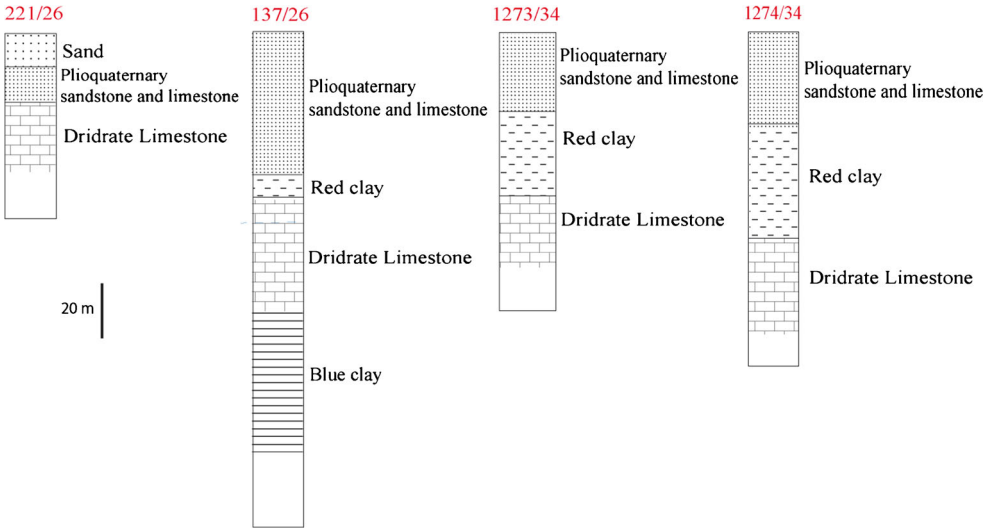

Fig. 2 Lithology of geological borehole of Oualidia

depression called Oulja. It is dominated by a quaternary cliff from which extends a rocky soil, mainly naked and without drainage network. The soil is composed of consolidated Plioquaternary dunes, arranged parallel to the coast with altitudes between 100 and 150 m (Fig. 3). The lagoon of Oualidia extends to the North of Oulja and is separated from the ocean by a consolidated dunes barrier (Bidet and Carruesco 1982).

Major geomorphological structures found in the region of Oualidia, from downstream to upstream, are as follows:

- Oulja: This is a depression limited from the hinterland by Plioquaternaire abandoned cliff and from the ocean by the Atlantic coast dunes. It extended from south to north, allowing large amount of seawater penetration, giving birth to the lagoon of Oualidia (Ouadia 1998).
- Abandoned cliff: It corresponds to abandoned shoreline with measured altitudes of 5, 20, and 30 m (Gigout 1951; Ouadia 1998). This is the barrier which separates the Oulja to the hinterland.
- The hinterland: is characterized by Pliocene and Quaternary sandstone consolidated dune relief, parallel to the ocean, with a SSW-NNE orientation (Abou Maria 1993).

Hydrogeology and piezometry

The piezometric map of May 2011 period has been prepared using data from 40 wells capturing the Plioquaternary in the area between El Oualidia and El Akarta (Fig. 4). Piezometric curves are generally parallel to the coast. The groundwater

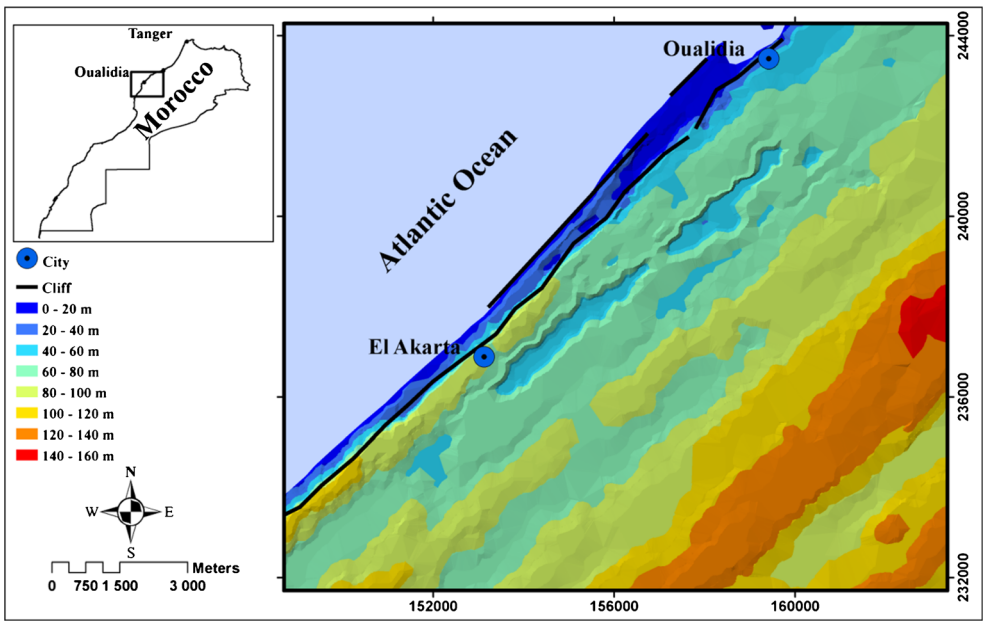

Fig. 3 Digital elevation model made from the Oualidia topographic map (Scale 1/50,000) showing the region geomorphology

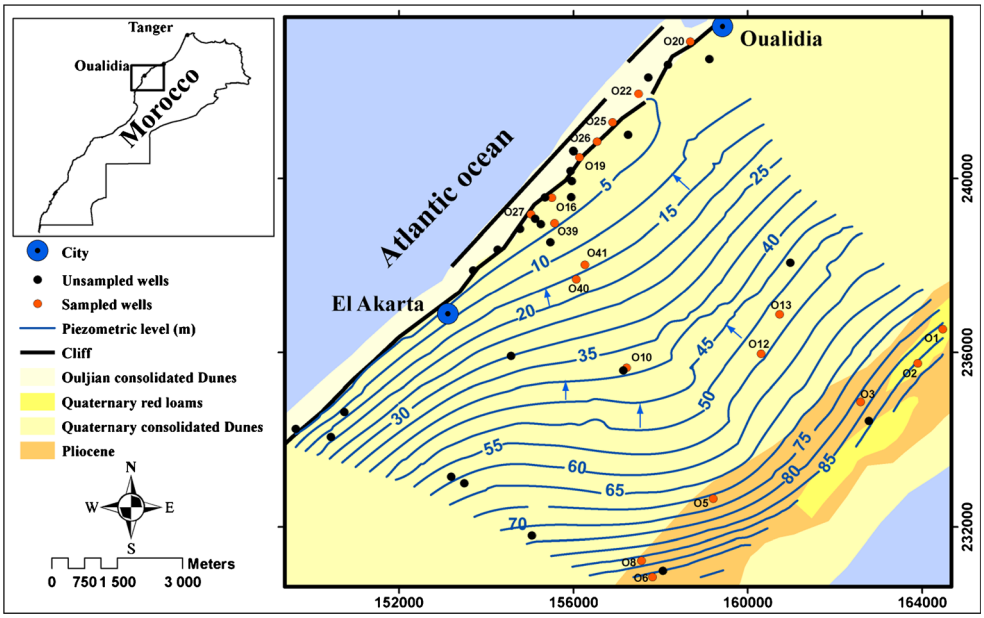

Fig. 4 Piezometric map of the study area

flow is toward the ocean, from the south-east to north-west. A drainage line was observed in the middle of the map. This structure was also observed on the piezometric maps of 1992 and 2003 (Fadili 2014). It was probably caused by the topography or a network karst effect which would drain the groundwater (Hilali 2002; Gilli et al. 2008).

This map shows two main hydrodynamic regions. The first is located in the south-east and characterized by slightly constricted piezometric lines, with calculated hydraulic gradient of 1.67 %. The second is located in the north-western, near the ocean, materialized by spaced piezometric lines and a low hydraulic gradient of 0.62 %. In the south of El Akarta, the piezometric curves are constricted with a high hydraulic gradient of 2.5 %. This is the consequence of the aquifer wall ascent and the low permeability.

Table 1 Physicochemical characteristics of the groundwater from wells

Wells	Distance from the Ocean (m)	Water depth (m)	Na (mg/l)	K (mg/l)	Mg (mg/l)	Ca (mg/l)	Cl (mg/l)	Br (mg/l)	NO_3 (mg/l)	HCO_3 (mg/l)	SO_4 (mg/l)	EC (mg/l)	pH	T (°C)
O19	490	4	654.1	30.3	290.9	591.7	1,416.9	3.6	53.7	345.7	20.3	5.8	7.06	21.7
O25	510	3.2	675.4	32.5	321.9	639.9	1,508.3	3.9	47.8	265.5	19.7	6.21	7.15	22.2
O27	534	29.2	566.4	22.2	338.1	320.5	1,242.2	3.5	89.0	189.9	22.4	4.79	7.48	22.2
O26	544	6.9	558.0	26.1	265.1	467.8	1,190.0	3.1	73.9	370.1	21.0	5.08	7.21	22.5
O20	600	6	632.4	26.7	287.6	640.0	1,410.2	3.7	24.0	223.3	20.8	5.91	6.97	22.9
O22	607	4.9	919.4	40.1	406.4	735.0	2,010.7	5.4	86.0	210.5	18.5	7.94	7.01	22.1
O16	622	23.15	553.6	25.1	244.8	507.4	1,199.9	3.1	39.0	255.4	21.0	5.07	7.05	22.9
O39	1,073	67.4	230.0	10.7	82.5	232.8	609.9	1.5	39.0	231.2	421.7	2.85	7.39	21.2
O41	2,309	62.3	187.4	8.6	63.6	193.3	414.1	1.0	79.4	211.0	362.2	2.14	7.46	21.9
O40	2,394	48	114.0	7.6	25.1	145.1	270.1	0.6	69.9	281.1	149.3	1.31	7.84	21.8
O10	4,648	21.72	34.4	8.6	10.9	63.4	37.9	0.1	47.1	225.3	41.8	0.33	7.69	27
O13	6,338	75.4	23.0	1.8	3.2	80.7	56.8	0.1	26.9	194.4	10.1	0.33	7.67	26.8
O12	6,689	63.8	27.4	2.1	3.7	80.1	52.8	0.1	27.1	233.6	20.3	0.31	7.69	27
O8	8,003	24.1	34.3	1.2	4.2	83.9	66.9	0.2	25.9	110.7	19.5	0.33	7.59	26
O5	8,166	50.92	35.9	3.6	6.9	84.8	79.0	0.2	98.4	195.1	22.1	0.26	7.8	23
O6	8,480	5	36.4	2.5	4.8	111.5	71.1	0.1	45.0	213.5	44.0	0.67	7.49	21.6
O3	9,028	11.56	29.1	7.1	2.8	62.6	41.3	0.1	35.2	191.7	25.2	0.19	7.8	25
O2	9,089	6.18	26.2	2.7	2.9	72.0	47.8	0.1	36.5	187.6	23.0	0.45	7.91	21.6
O1	9,440	5.78	32.9	1.8	3.6	90.6	62.7	0.2	30.8	190.1	19.4	0.58	7.41	21.5

Materials and methods

Sampling and hydrochemical analysis

In this study, freshwater was taken as rainwater concentrations and samples were taken from 19 wells during a high water period (May 2011). The sampled wells are located, as far as possible, in a profile perpendicular to the coast line (Fig. 4). Hydrochemical analyzes (Table 1) were performed in the I2M UMR 5295 Laboratory at the University of Bordeaux, by the ion chromatography method. This method was used to determine the concentrations of major elements: Na^+, K^+, Mg^{2+}, Ca^{2+}, Cl^-, and Br^-. Some physicochemical parameters were measured in situ, such as water temperature, electrical conductivity (EC), and pH. Bicarbonates were also titrated in situ by the volumetric method on 100 ml of water using sulfuric acid (H_2SO_4 1 N) as a titrand.

Geophysics

Six electrical resistivity tomography profiles (ERT profiles: W1, W2, W3, W4, D1, and D2), perpendicular to the shore in the NW-SE direction, were carried out in the region to detect seawater intrusion extension from the edge of the coast to the hinterland (Fig. 5). The first four profiles (W1, W2, W3, and W4) were located in the sandy depression (Oulja) with Wenner array type. The two other profiles (D1 and D2) were located beyond the Plioquaternary cliff, on rocky area with dipole-dipole array type. The acquisition was performed by the Syscal Junior menu of 72 electrodes placed at intervals of 5 m; the length of each profile is 355 m. Data inversion was carried out by Res2Dinv software using L1 robust inversion (Loke and Barker 1996).

For the geophysical prospection investigation in hydrogeology, the aim was to define parameters associated directly or indirectly to the groundwater aquifer and the measured resistivity (Guerin 2004). Archie (1942) proposed an empirical formula (Eq. 1) which permit determining the electrical resistivity of an aquifer formation:

$$\rho_f = a\varphi^{-m}S^{-n}\rho_w \tag{1}$$

With: ρ_f the formation resistivity (Ω m), ρ_w the water resistivity (Ω m), φ the formation porosity (dimensionless), S the saturation, and a, m, n are respectively the coefficient of saturation that depends on lithology ($0.5 \leq a \leq 2.5$), cementation factor which depends on the pore shape and the rock compaction and varies between 1.3 and 2.2 for unconsolidated cemented limestone sands, and saturation exponent which is close to 2.

However, for better calibration of the ERT data, electrical profiles were calibrated by mechanical borehole and by Archie formula, knowing the formation porosity and groundwater electrical conductivity.

Results and discussion

General hydrochemistry of groundwater

Table 2 showed statistical summary of concentrations of analyzed major ions. Samples groundwater EC ranges from 0.2 to 7.9 mS/cm with an average of 2.7 mS/cm higher than the median of 1.3 mS/cm. The pH is between 7.0 and 7.9 with a mean value of 7.5 which equals to the median (Table 2).

Fig. 5 Localization of electrical resistivity tomography profiles

Table 2 Statistics summary of chemical elements

	Na (mg/l)	K (mg/l)	Mg (mg/l)	Ca (mg/l)	Cl (mg/l)	Br (mg/l)	NO_3 (mg/l)	HCO_3 (mg/l)	SO_4 (mg/l)	EC (mS/cm)	pH
Minimum	23.0	1.2	2.8	62.6	37.9	0.1	24.0	110.7	10.1	0.2	7.0
Maximum	919.4	40.1	406.4	735.0	2,010.7	5.4	98.4	370.1	421.7	7.9	7.9
Average.	282.6	13.8	124.7	273.9	620.5	1.6	51.3	227.7	68.5	2.7	7.5
Median.	114.0	8.6	25.1	145.1	270.1	0.6	45.0	213.5	21.0	1.3	7.5
Standard deviation	303.7	12.7	148.5	240.0	668.6	1.8	24.0	58.5	118.2	2.6	0.3

Major ions concentrations showed that most dominant anions are Cl^- and HCO_3^- and the most dominant cations are Ca^{2+} and Na^+ in the groundwater. The Cl^- concentrations are between a minimum of 37.9 mg/l and a maximum of 2,237.9 mg/l with an average of 620.5 mg/l higher than the median of 270.1 mg/l. Bicarbonates HCO_3^- concentrations varies from a maximum of 370.1 mg/l and a minimum of 110.7 mg/l with an average value of 227.7 mg/l slightly above the median which equals to 213.5 mg/l. The Ca^{2+} concentrations are between 62.6 and 735.0 mg/l; the average is equal to 620.5 mg/l and higher than the median of 270.1 mg/l. The sodium concentration is ranging from 23.0 to 919.4 mg/l with an average value of 282.6 mg/l and a median of 114.0 mg/l.

The carbonate nature of the aquifer may be the possible source of calcium and bicarbonate in groundwater. The presence of Cl^- and Na^+ in groundwater can be from seawater origin as will be detailed later. The most important source of sulfate in water is the dissolved evaporite as gypsum ($CaSO_4 \cdot 2H_2O$) and anhydrite ($CaSO_4$). The SO_4 concentration is between 10.1 and 421.7 mg/l.

Electrical conductivity of the Plioquaternary Groundwater

Water EC represents the salinity degree, which is a linear function of dissolved ions (Meybeck 1987). The EC measures were performed on site with a conductometer (Hanna HI 9828).

The EC map represented in Fig. 6 was obtained by the data interpolation of 40 wells distributed on the studied area. The map showed that the highest conductivities are observed at the coast fringe. To inland, conductivities become weaker. This suggests the existence of seawater intrusion being responsible for groundwater salinization near the ocean. Indeed, it has been reported that along the coastline, the high values of EC are generally attributed to the seawater intrusion (Stamatis and Voudouris 2003).

Toward the south of El Akarta, EC become weaker despite the proximity of the ocean. This may be the consequence of the Plioquaternaire base level ascend. In contrast, it was collapsed between Oualidia el Akarta. This observation may be explained by the high value of the piezometric gradient (Fig. 4), the low number of wells, and the low aquifer exploitation in this part.

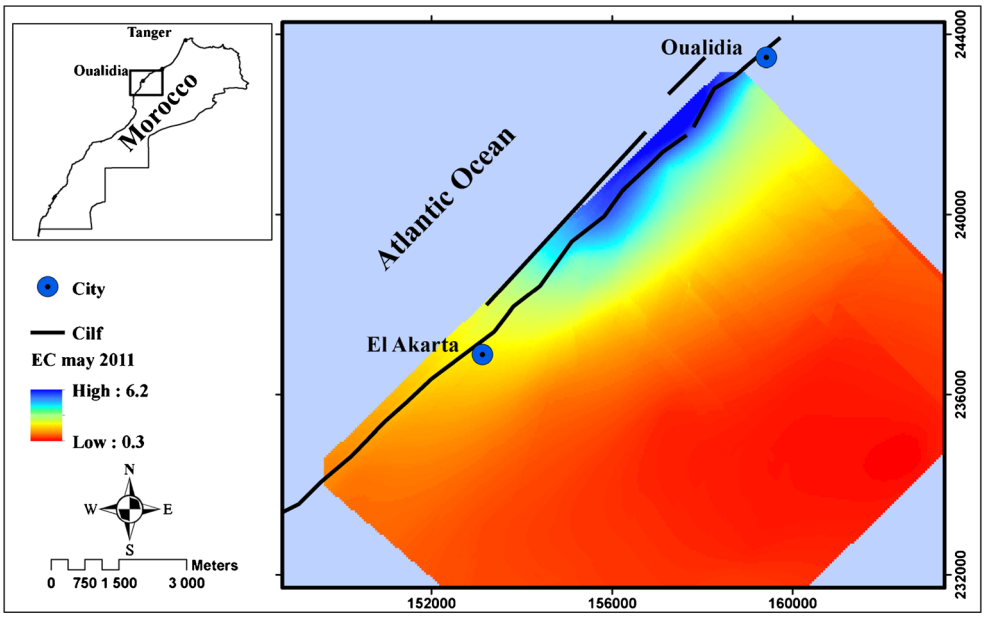

Fig. 6 EC map of the study area (May 2011)

Chemical facies of groundwater

To identify the hydrochemical facies of groundwater, results are presented in Piper diagram (Fig. 7) based on anions and cations concentrations. The Piper diagram realization was made using the software Diagrammes (Simler 2004). The facies of all wells located in the first 2 km from the ocean are of Cl-SO_4-Ca and Cl-SO_4-Na facies. Wells located beyond 2 km perpendicular to the ocean have a Ca-HCO_3 facies. Moving from the closest well to the ocean to the far one, the cations diagram indicates a migration from Na-facies to Ca-facies. As regards the anions diagram, it can distinguish two groups. The first is characterized by a Cl-SO_4 facies for the wells located in the first 2 km, and a second group is characterized by a HCO_3 facies for the far wells.

However, Piper diagram indicate a facies change, mainly due to the distance from the ocean as well as the morphology variation.

Over all, the facies of water is modified due to the influence of several factors: interaction between water and aquifer material mainly carbonated, and the influences of human activities such as the return of flow irrigation and overexploitation of the aquifer system. The increase of sodium, sulfate and chloride concentration, from fresh water to seawater (mixing line), indicates the influence of the seawater on the aquifer facies.

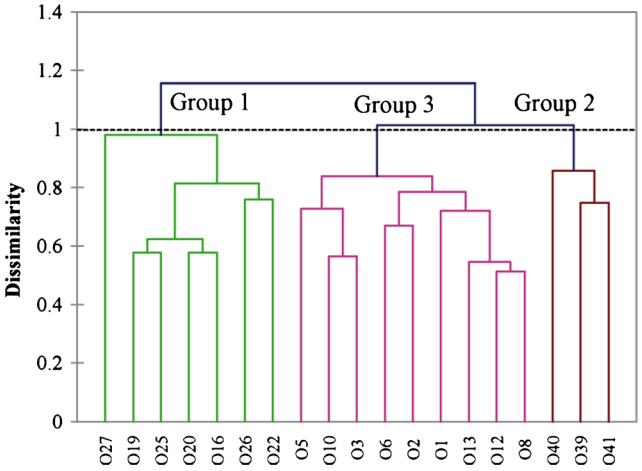

Fig. 8 Hierarchical classification data of the wells in Oualidia

Relationship between chemical elements and groundwater mineralization processes

The analysis by ascending hierarchical classification aims to classify the observation into groups according to similarities and differences between them. It successively joins the most similar observations with respect to the gravity center (Davis 1986). This classification was performed by Ward method with the Euclidean distance. The result showed the existence of three main groups (Fig. 8). The first group of water has high conductivity in the range of 4.8 to 7.9 mS/cm, with an average

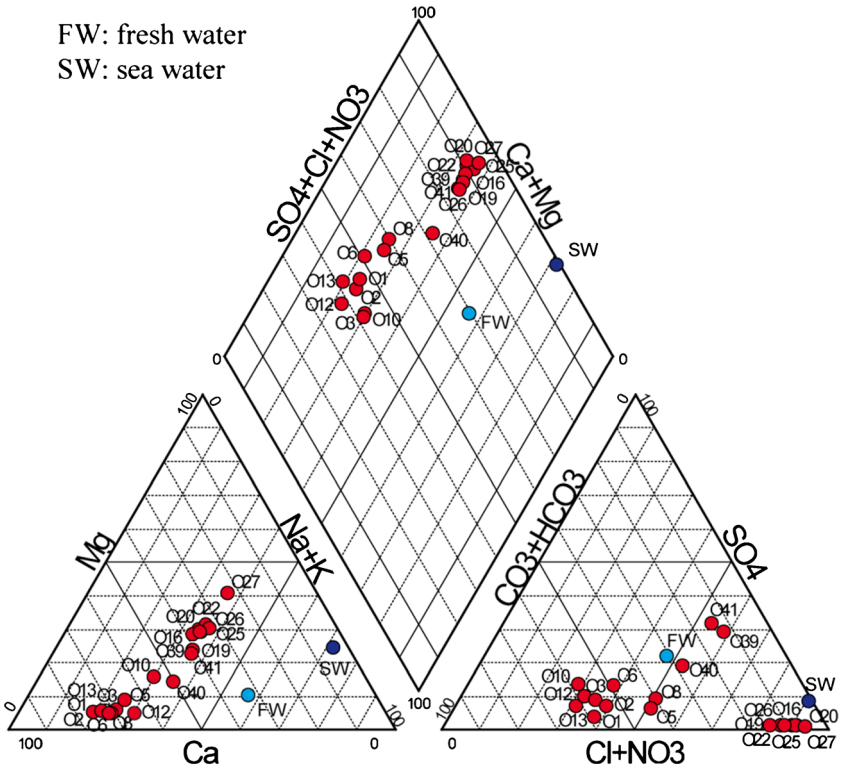

Fig. 7 Piper diagram representation of chemical facies of Oualidia groundwater

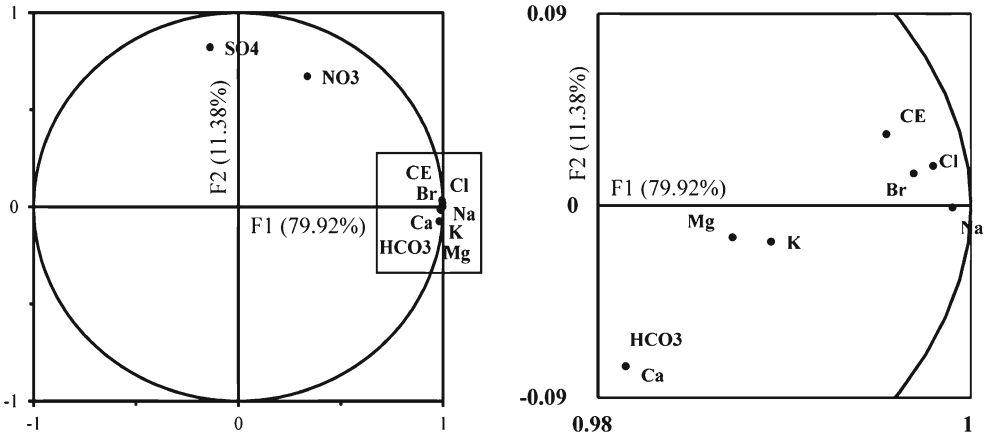

Fig. 9 Variables correlation circle on the F1-F2 factorial plane

of 5.8 mS/cm. These waters are characterized by Na^+ (651.3 mg/l on average) and Cl^- (1,425 mg/l on average) abundance. The first group wells are located in a morphological unit called Oulja at a distance not exceeding 1 km of the ocean. The second group presents means EC between 1.3 and 2.9 mS/ cm, with an average value of 2.1 mS/cm. The most abundant ions in this group are HCO_3^- (241.1 mg/l on average) and Ca^{2+} (190.4 mg/l on average). The wells of the second group are located between 1 and 2 km to the ocean. The third group is characterized by low electrical conductivity, ranging from 0.2 to 0.7 mS/cm, with an average of 0.4 mS/cm. This group is characterized by the abundance of HCO_3^- ions. The third group wells are located in the hinterland beyond 2 km from the ocean.

Principal component analysis is a method of multivariate data analysis used to reveal trends in large data sets (Winter et al.; 2000; Chen et al.; 2007; Choi et al. 2014; Masoud 2014). The variables (major ions) projection on the F1-F2 factorial plane (Fig. 9) shows that the F1 axis which expresses 79.92 % of the total variance is mainly determined by the electrical conductivity, Na^+, Cl^-, K^+, Ca^{2+}, Mg^{2+}, Br^-, and HCO_3^-. Thus, it represents the axis of mineralization. The vertical axis, F2, expresses 12.52 % of the total variance and determined, in a positive manner, only by SO_4^{2-} and NO_3^-. However, it shows the sulfates and nitrates pole.

The projection of individuals (sampled wells) on the F1-F2 factorial plane (Fig. 10) revealed that the F1 axis shows opposition between the weakly and the highly mineralized waters. Weakly mineralization waters (group 2 and group 3) are located in the upstream of the aquifer, beyond 1 km of the ocean. Highly mineralized waters (group 1) are located in Oulja at 1 km of the ocean. Also, F2 axis showed an opposition between waters rich in SO_4^{2-} and NO_3^-, and waters weakly charged by these elements (Fig. 10).

In summary, the first group wells are the most mineralized with facies mainly sodium and chloride type, which could be a marine effect consequence. The wells of the second group indicate a migration to the nitrates and sulfates pole which is the result of crop agriculture activities effect.

The ionic relationships study permit to explain the different hydrogeochemical mechanisms involved in the groundwater mineralization. The representation of $Ca^{2+}+Mg^{2+}$ in function of $HCO_3^-+SO_4^{2-}$ (Fig. 11) shows that most points of the first

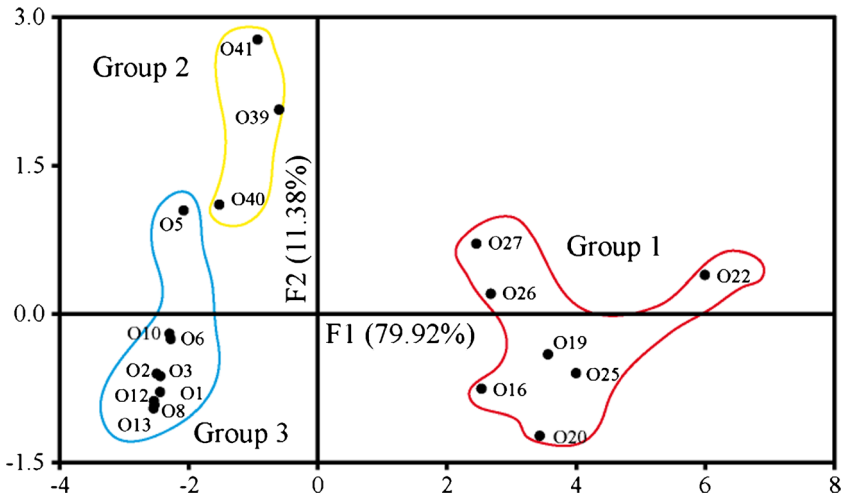

Fig. 10 Individuals diagram on the F1-F2 factorial plane

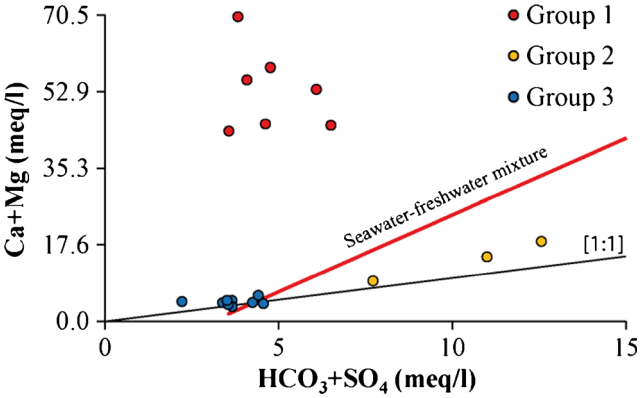

Fig. 11 Graphic of $Ca^{2+}+Mg^{2+}$ versus $HCO_3^-+SO_4^{2-}$

group are above [1:1] line, indicating that the ion exchange, as a result of seawater intrusion, could be the process responsible for the enrichment in Ca^{2+} and Mg^{2+} in favor of $HCO_3^-+SO_4^{2-}$ (Cerling et al. 1989; Fisher and Mullican 1997; Wanda et al. 2011). Second and third group samples are aligned on the [1:1] line, which suggests that Ca^{2+}, Mg^{2+}, HCO_3^-, and SO_4^{2-} ions are derived from the calcite, limestone, and gypsum dissolution, indicating aquifers lithology effect in the area (Belkhiri et al. 2012;. Nasher et al. 2013; Khairy and Janardhana 2013; Han et al. 2014; Srinivasamoorthy et al. 2014).

The Na/Cl ratio is often used to identify the mechanisms of groundwater mineralization (Magaritz et al. 1981; Dixon and Chiswell 1992; Sami 1992; Mtoni et al. 2013). If the halite (NaCl) dissolution is responsible for the sodium presence in the water, the ratio will be equal to 1. A ratio greater than 1 indicates Na^+ release from the clay matrix (Meybeck 1987). In this case, the samples have abundance in HCO_3^- (Stallard and Edmond 1987; Rogers 1989; Mtoni et al. 2013). The Na/Cl ratios in the case of seawater intrusion are generally lower than the seawater ratio (i.e., <0.86, molar ratio) (Jones et al. 1999; Rao and Rao 2009; Reddy 2013).

In this study, Na/Cl molar ratio is between 0.6 and 1.11 with an average of 0.8 (Fig. 12). Two samples have a ratio greater than 1 (O10 and O3) with an abundance of HCO_3^- ions (197.7 mg/l for O3 and 225.3 mg/l for O10). This result indicates that the silicate weathering is responsible for these two wells enrichment by sodium. The ratio is less than 1 in most samples, reflecting that the enrichment in sodium is caused by the marine influence; mainly in the first group samples which are close to the ocean.

The correlation between the sum of anions Cl^- and SO_4^{2-} and the sum of cations Na^+ and K^+ (Fig. 13) showed that the first group present high chloride concentration suggesting saltwater intrusion. However, the second and third groups showed a low Cl^- concentration, which suggests freshwater and aquifer interaction. The abundance of Cl^- and Na^+ in the first group is the result of seawater intrusion, while SO_4^{2-} and Ca^{2+} ions indicates a water-rock interaction trough the gypsum dissolution which is derived from deep gypsiferous formations (Srinivasamoorthy et al. 2014). These formations may also present a mineralization source of Plioquaternary groundwater (Kaid rassou et al. 2005).

Nitrates are mainly issued from the anthropic activities, leachate, agriculture, domestic wastewater (Park et al. 2005; Kass et al. 2005; Schiavo et al. 2006). The nitrates concentration in groundwater of the area range from 24.0 to 98.4 mg/l. To investigate fertilizer as probable source of potassium and nitrate in groundwater, the concentration changes of these elements were plotted in the Fig. 14. The graph showed nitrate enrichment relative to potassium with simultaneous increase of both ions. This is the consequence of water K^+ fixation by clay minerals and release of NO_3^- (Nasher et al. 2013), demonstrating nitrates contamination of groundwater issued from anthropic activities (Dutta et al. 1997; Kumar et al. 2006; Reddy 2013).

To understand groundwater mineralization process against seawater intrusion, the graphs showing the relationship between the major elements (Ca^{2+}, Mg^{2+}, Na^+, K^+, Br^-, and SO_4^{2-}) of 19 wells and Cl^- were represented (Fig. 15). However, chlorides have conservative tracer, which participate neither in water-rock interactions, nor in redox reactions and does not form insoluble precipitate (Fetter 1993). They characterize

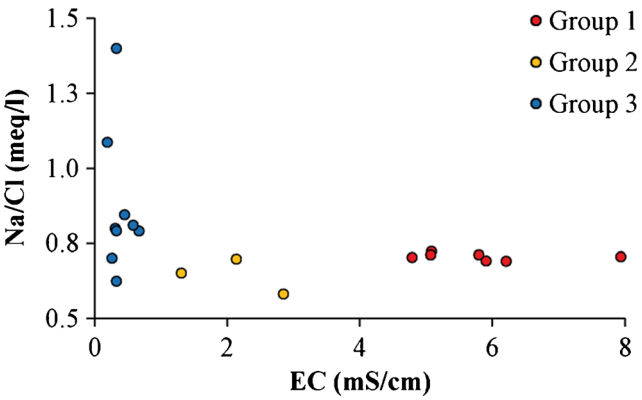

Fig. 12 The Na/Cl ratio versus EC

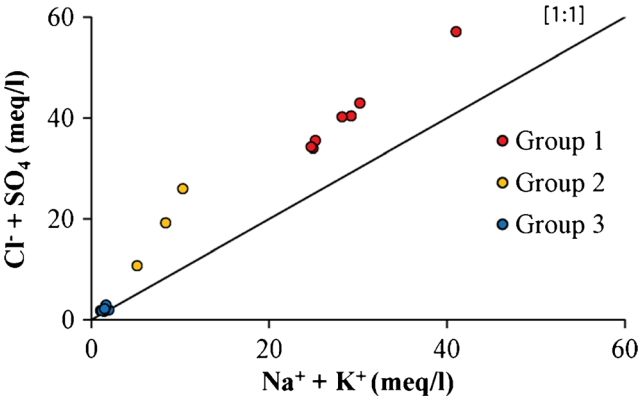

Fig. 13 The correlation between $Cl^-+SO_4^{2-}$ and Na^++K^+

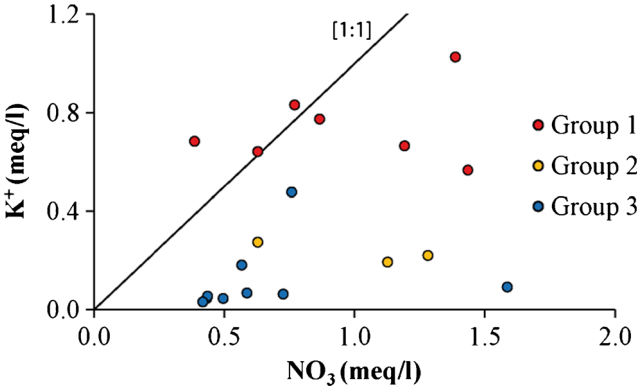

Fig. 14 Representation of NO_3^- versus K^+

the water salinity origin and form a mixture tracer (Tellam 1995; Fidelibus and Tulipano 1996; Rajesh et al. 2012; Ako et al. 2012; Re et al. 2013; Xing et al. 2013).

In general, sampled water showed a Ca^{2+} enrichment and Na^+, K^+, and Br^- depletion. The enrichment or depletion of major elements in groundwater is due either to Ca^{2+} and Mg^{2+} exchange under the interaction between water and carbonated rock, or to Na^+-Ca^{2+} or Na^+-Mg^{2+} reaction through basic exchange or sulfates reduction (Fidelibus and Tulipano 1996; Duriez et al. 2008; Fehdi et al. 2009; Belkhiri et al. 2012; Ako et al. 2012; Xing et al. 2013).

The graph of Na^+ in function of Cl^- indicated that all points are located below the mixture line. This phenomenon is explained by the ion exchange between water and aquifer which leads to Na^+ fixation and Ca^{2+} release. This is observed in the figure representing Ca^{2+} versus Cl^- (Fig. 15), which showed that all points are above the mixture line. This is the consequence of Na^+ fixation and Ca^{2+} release (Fidelibus and Tulipano 1996; Duriez et al. 2008; Giambastiani et al. 2013; Han et al. 2014; Srinivasamoorthy et al. 2014).

The graph of Mg^{2+} showed dispersion around the mixture line, with depletion in the wells distant from the ocean and enrichment in those close to the ocean (Fig. 15). In carbonated environment, such as the area under study, the water-rock interaction or dolomitization is the Mg^{2+} depletion cause (Tulipano and Fidelibus 1984; Fidelibus and Tulipano 1986; Duriez et al. 2008; Fehdi et al. 2009; Rajesh et al. 2012).

The plots of K^+ and Br^- in function of Cl^- (Fig. 15) showed that all points are located below the mixture line, except for a few points of potassium (K^+), showing an origin probably

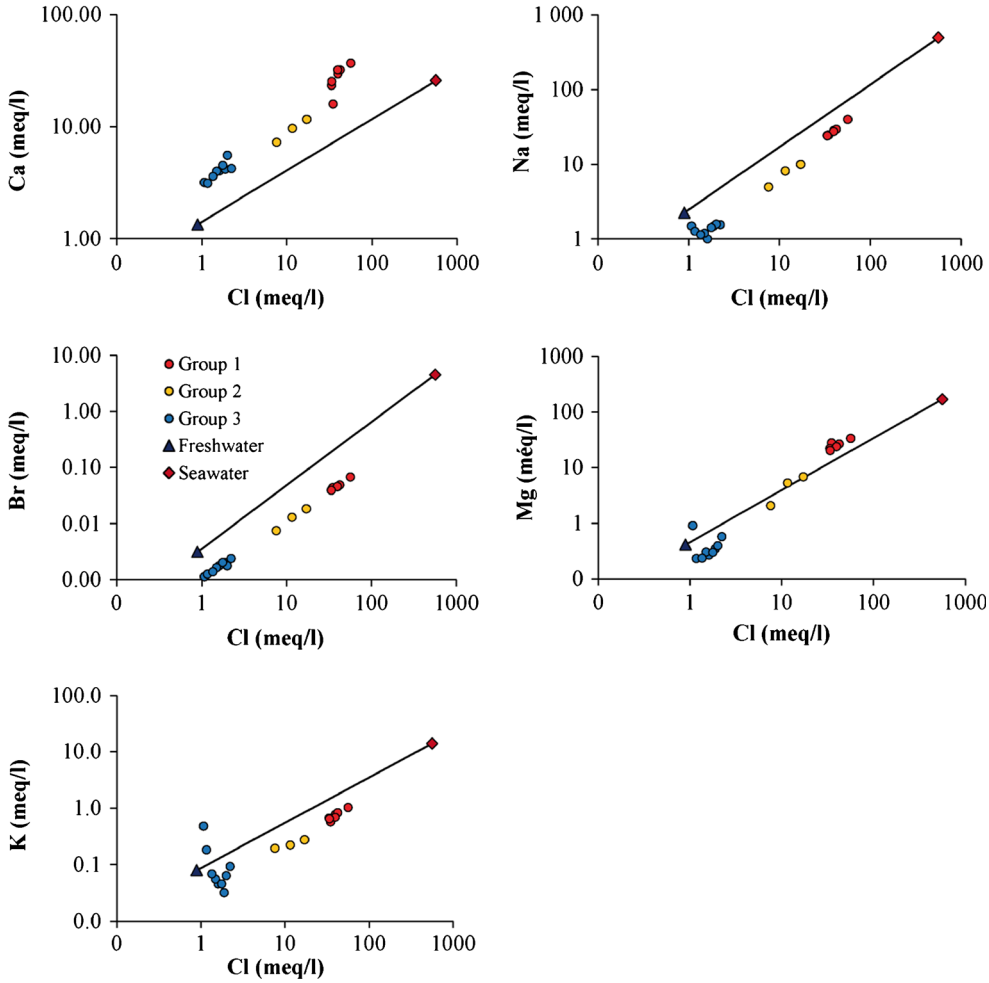

Fig. 15 Relationship between Br^-, Na^+, Mg^{2+}, Ca^{2+}, K^+, and Cl^-

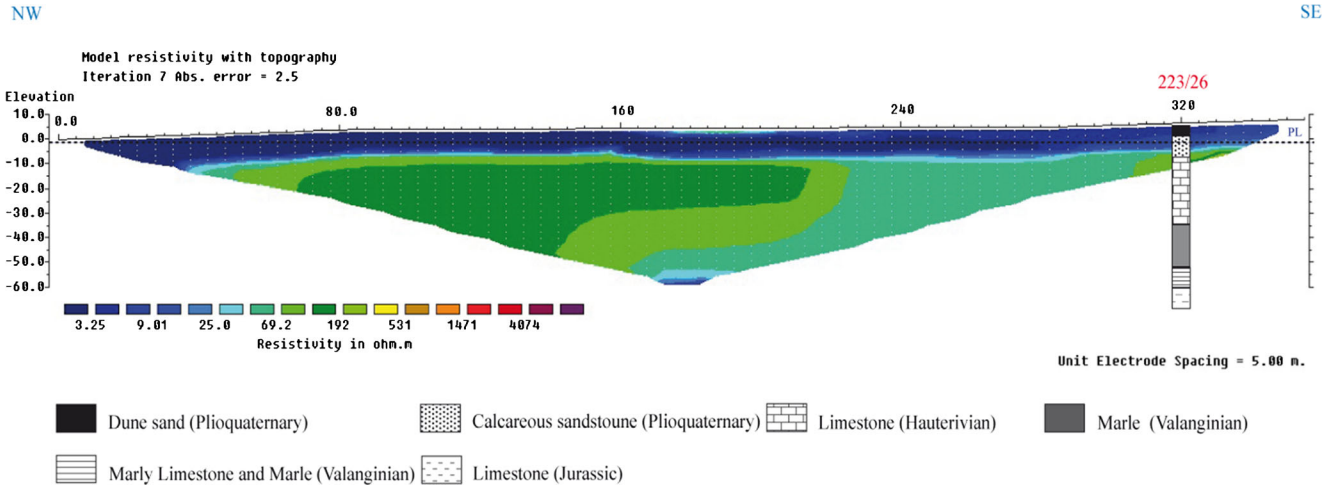

Fig. 16 Profile of electrical resistivity tomography W1

oceanic for these elements mainly for the wells close to the coast. Consequently, K^+ depletion is the result of NO_3^- release as it has been showed above (Fig. 14).

From the graphs of Fig. 15, it was noticed that the wells closer to the ocean are mineralized and tends toward the seawater mineralization, while the distant ones present a mineralization close to the freshwater. This is another indicator of oceanic effect in these wells.

In summary, the Plioquaternary groundwater of Oualidia presents two sources of mineralization. One first source is through the interaction between groundwater and carbonated rock. The second one is by ionic exchange under seawater intrusion effect, mainly for wells located in the Oulja.

ERT profiles interpretation

Based on the results obtained by hydrochemical study, six ERT profiles were performed on the two highlighted areas (Fig. 5). Four profiles at the Oulja, the area which present mineralization mainly due to ion exchange under the seawater intrusion effect. Two profiles beyond the Plioquaternary abandoned cliff, where mineralization is mainly due to water-aquifer interaction. Then, the purpose was to determine seawater intrusion extension.

The ERT profiles data were calibrated on geological borehole taking into account water EC of the closest wells.

The profile W1 (Fig. 16) was performed at 179 m of the ocean. The obtained resistivity along the profile at 10 m depth ranged from 1 to 20 Ω m. This low resistivity corresponds in part to a marshy area and aquifer saturated by brackish water. The measured EC in the well O22, which is close to the profile, is 6.15 mS/cm measured at 5.4 m depth and well correlated to the conductor roof. The porosity of Oualidia coastal aquifer formations varies between 10 and 20 %, with a minimum of 15 % for Plioquaternary deposits (DRHT-FAO 1994). The apparent resistivity calculated by Archie formula (Eq. 1),

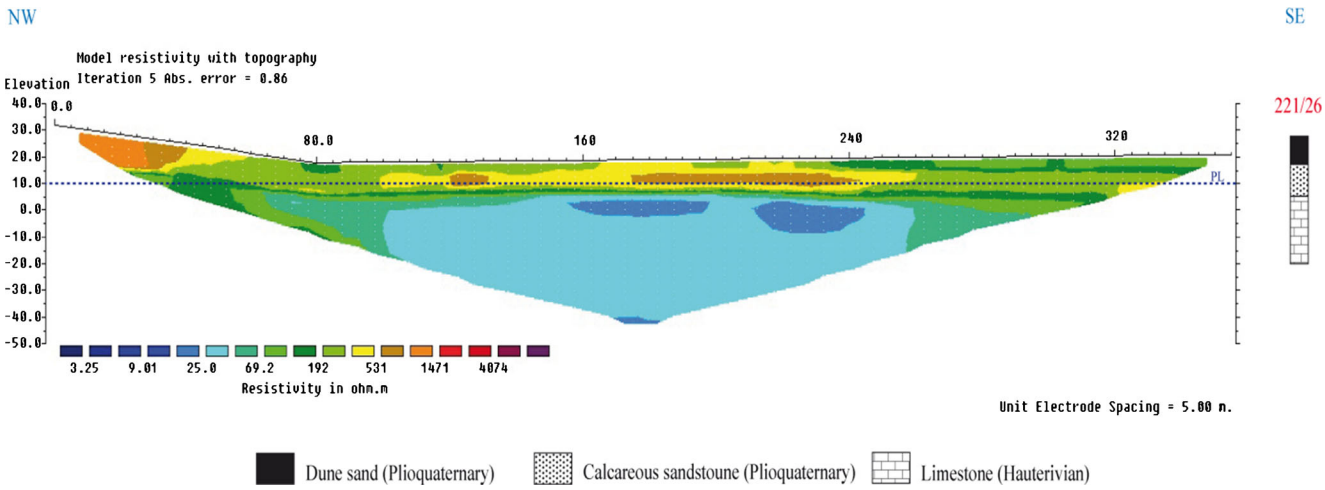

Fig. 17 Profile of electrical resistivity tomography W2

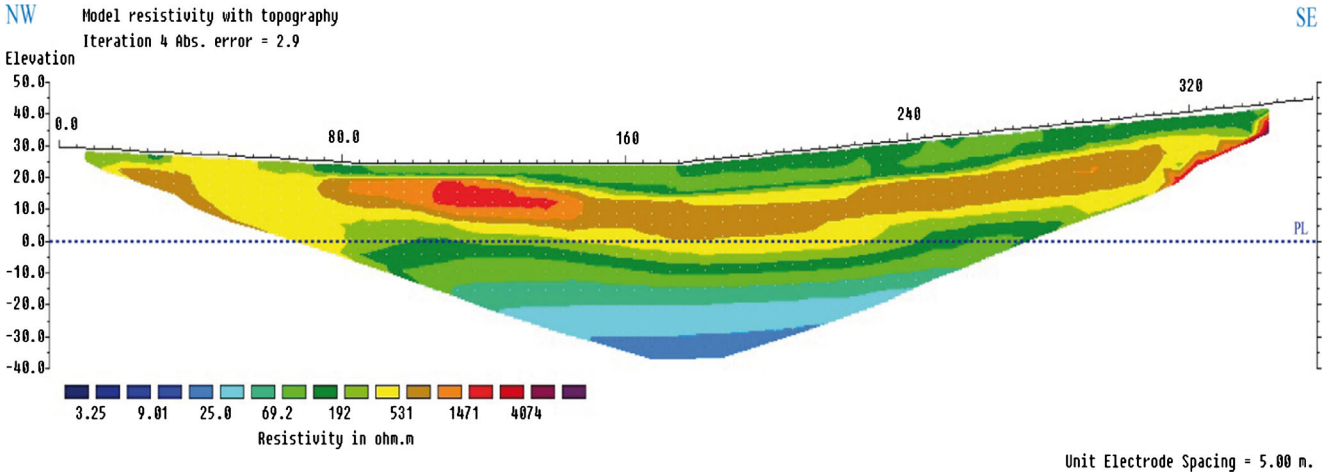

Fig. 18 Profile of electrical resistivity tomography W3

taking into account the porosity of the aquifer and EC of the well O22, shows resistivity from 2.4 to 9.2 Ω m which is consistent with the resistivity values obtained by this profile.

The correlation of W1 profile with the borehole 223/26 shows that the conductor level (1 to 20 Ω m) accords with Plioquaternary aquifer encroached by seawater at 10 m depth. Below this level, resistivity between 20 and 70 Ω m is attributed to the Hauterivian aquifer with brackish water. At the profile platform, the conductor level whose resistivity varies between 10 and 30 Ω m at 45–50 m depth corresponds to blue clay observed at the end of borehole 223/26.

The profile W2 (Fig. 17) was performed at 180 m perpendicular to the coastal fringe. The profile interpretation revealed a high resistant level at 20 m depth with resistivity ranging from 100 to 700 Ω m; and a lower conductor level whose resistivity varies between 10 and 25 Ω m. Comparing the profile (W2) with the lithology of the borehole 221/26 indicates good correlation, allowing to attribute the high level to unsaturated Plioquaternary formation and the lower level to Plioquaternary aquifer and Hauterivian limestone encroached by seawaters. The depth of the conductor level on the profile corresponds to the water depth measured at the well O16 which is 23.2 m, with an EC of 5.2 mS/cm. Based on the Archie formula calculation and the porosity given by DRHT 1994, cited above, lower resistivities of 2.8 Ω m are obtained for a porosity of 20 %, 4.8 Ω m for a porosity of 15 %, and 10.6 Ω m for a porosity of 10 %. These resistivities characterize the water salinization.

The profile W3 (Fig. 18) was performed perpendicularly and at a distance of 100 m from the coast. The interpretation of this profile shows resistant formations at the surface (between 70 and 1,500 Ω m) up to 40 m deep, followed by a conductor level whose resistivity is between 25 and 70 Ω m. Due to the lack of lithological borehole near the profile, it is difficult to estimate the lithology. Analogically with lithology observed in other borehole, the first level may corresponds to the dry Plioquaternary sandstone. The upper part of the second level corresponds to the limestone Dridrate aquifer (late Hauterivian). The well O30 measured EC which is near the profile was 2.45 mS/cm, at water depth of 38 m. the water depth measured in the well corresponds exactly at the conductor depth on the profile. Integrating the porosities from 10 to

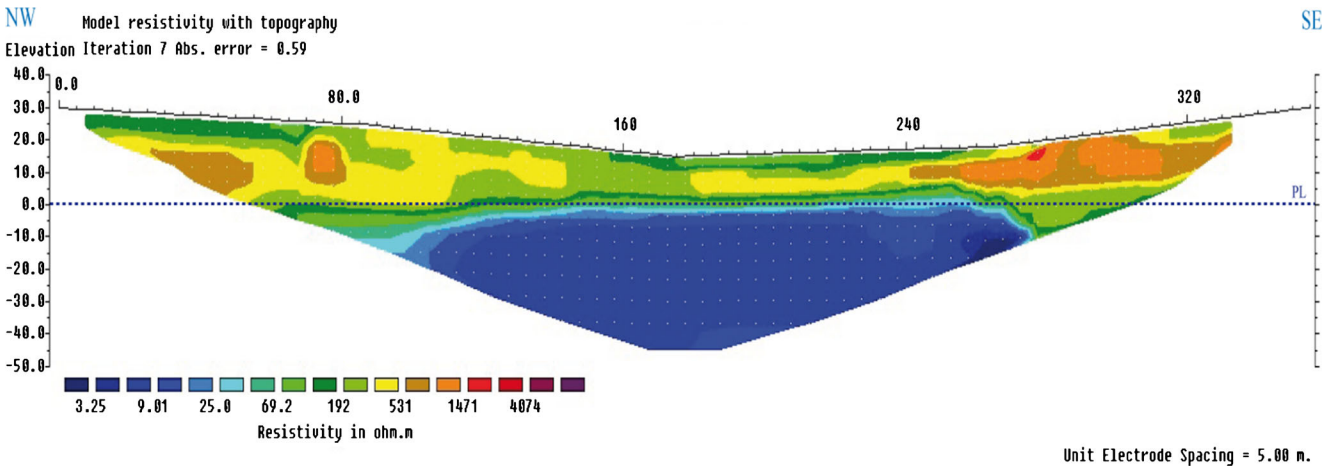

Fig. 19 Profile of electrical resistivity tomography W4

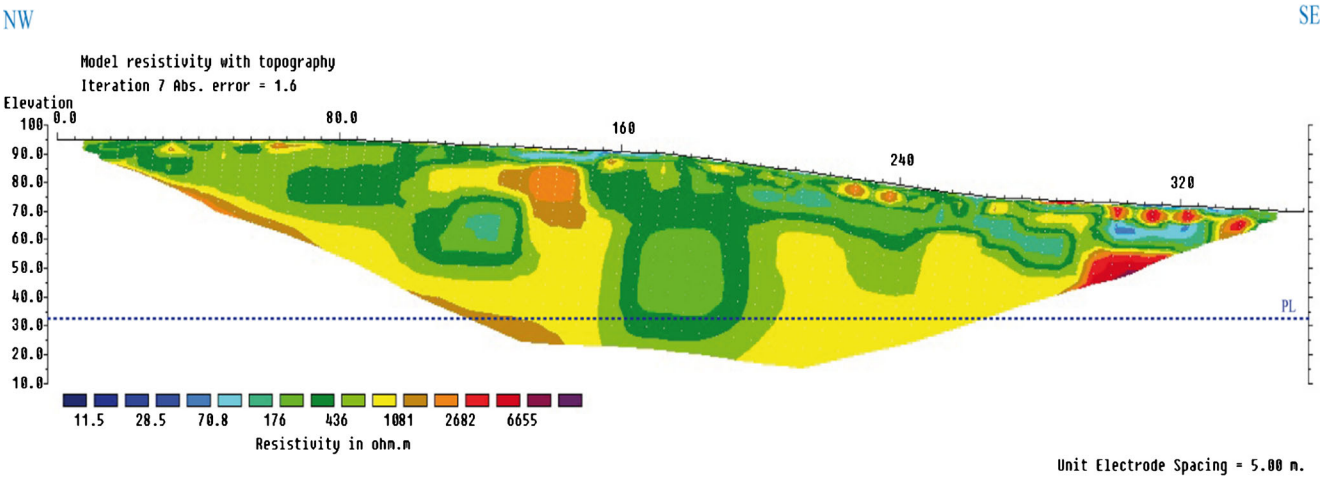

Fig. 20 Profile D1 of electrical resistivity tomography

20 % (DRHT 1994) and the measured EC in the well in the Archie equation, resistivities in the range of 6 to 22 Ω m were obtained, indicating that the aquifer in this area is saturated with brackish water.

Profile W4 (Fig. 19) was performed at 200 m perpendicularly to the coast. This profile was located at the southern of the Oulja. It shows high resistivities level ranging from 70 to 700 Ω m up to 30 m depth, followed by a conductor level whose resistivity varies between 3 and 20 Ω m. The upper level corresponds to a sandy filling and dry Plioquaternary sandstone. The water EC measured in the well O34 near the profile is 1.7 mS/cm at 30.2 m depth, which corresponds to W4 profile conductor roof. The apparent resistivity calculated based on Archie formula, considering porosities described by DRHT (1994), varies from 8 to 32 Ω m, indicating the presence of brackish-salt water in the aquifer. The conductor level is attributed to the Plioquaternary sandstones and Dridrate limestones aquifer (late Hauterivian) directly connected in this part and saturated with brackish-salt water.

The profile D1 was executed at 1 km from the coast (Fig. 20) beyond the Plioquaternary abandoned cliff. It shows high resistivity between 1,000 and 6,000 Ω m. The water depth measured in the well O38 near the profile is 50 m, with a low EC of 0.59 mS/cm characterizing the presence of freshwater. Resistant formations correspond to Plioquaternary sandstone and late Hauterivian Dridrate limestones. This profile does not show any influence of seawater on the Dridrate limestone aquifer.

The profile D2 was made at 1 km from the sea with dipole-dipole array (Fig. 21). The pseudo-section obtained after inversion shows resistivity that varies between 80 and 6, 000 Ω m. This resistivity fluctuation is due to the heterogeneous content of this formation. From 40 m depth, a resistant formation with a resistivity ranging between 1,000 and 6, 000 Ω m was encountered; which is corresponding to the late Hauterivian limestone.

In summary, in Oulja, where the two aquifers are directly connected, the water level corresponds to a decrease in

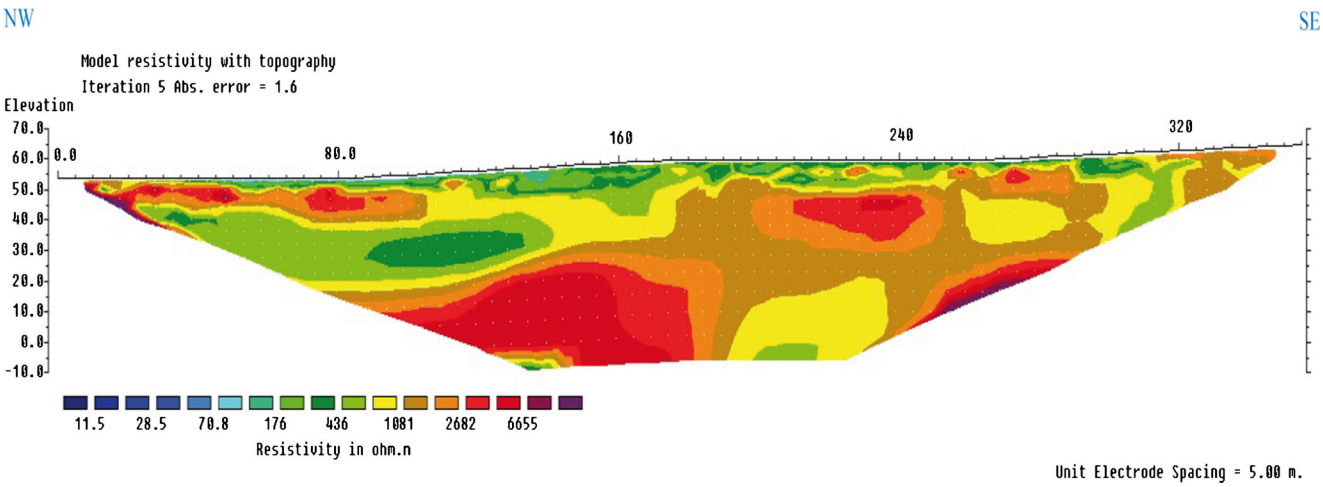

Fig. 21 Profile of electrical resistivity tomography D2

measured resistivity. Oulja is characterized by the presence of marshy and seawater intrusion. Tomographic profiles performed in the first kilometer perpendicular to the coast showed variable values of resistivity; one resistant level from 20 to 40 m thick with high resistivity ranging from 150 to 1, 000 Ω m, and one second conductive level with lower resistivity less than 30 Ω m. The upper resistant level observed on W2, W3, and W4 profiles becomes conductive with depth due to the presence of brackish-salt water that are related to seawater intrusion. The decrease in thickness of the resistant level from south to north, consequence of Oulja morphology decreasing altitude, involves the emergence to the surface of the conductive layer on the W1 profile.

ERT resistivity models beyond the Plioquaternary paleo cliff (D1, D2) (further than 1 km from the cost) show resistivity range different to that encountered in the Oulja. These profiles were characterized by very high resistivity attributed to Plioquaternary sandstone formation with high thickness up to 50 m, overlying Hauterivian limestones.

Conclusions

Geophysical and hydrochemical analysis were performed to evaluate groundwater mineralization and extension in the Oualidia area, where the groundwater flow is toward the Atlantic Ocean.

Geochemical analysis showed that the groundwater mineralization in Oualidia is conditioned by two factors; ion exchange under water-rock interaction and seawater intrusion effect. However, the spatial variation of salinity is dependent of the area morphology. In Oulja, near the coast, the mineralization was highest while decreasing gradually from 1,000 m of the ocean further than the Plioquaternary paleo cliff. This subdivision was justified by the principal component analysis. The first group of samples located in Oulja indicated significant mineralization level with the abundance of sodium and chloride facies type, indicating the seawater intrusion effect. The second and third groups of samples, located beyond the paleo cliff, present low mineralization level with abundance of calcium and bicarbonate facies type due to the interaction with the aquifer.

To justify hydrochemistry results, seawater intrusion extension was detected based on electrical resistivity tomography. After profiles calibration by lithological boreholes and Archie's formula, the results showed that the contamination effect shown by the conductive layer (resistivity lower than 30 Ω m) on the profiles remains limited to the Oulja area. The seawater intrusion effect disappears further on the hinterland as shown by resistivity models. Consequently, the electrical tomography confirmed the hydrochemical results in the region between El Oualidia and El Akarta, devoted to agricultural purposes. Over all, the seawater intrusion in the area between El Oualidia and El Akarta remains limited within 1 km from the ocean in the Oulja area.

References

Abou Maria K (1993) Les formations quaternaires du Sahel des Doukkala (Méséta occidental marocaine): mise en place et évolution post-sédimentaire. D.E.S., Thèse de 3 ème cycle, Fac. Sci, Rabat, 8 tab., 88 fig., 186 p

Agoubi B, Kharroubi A, Abichou T, Abida H (2013) Hydrochemical and geoelectrical investigation of Marine Jeffara Aquifer, southeastern Tunisia. Appl Water Sci 3(2):415–429

Ako AA, Shimada J, Hosono T, Ichiyanagi K, Nkeng GE, Eyong GET, Roger NN (2012) Hydrogeochemical and isotopic characteristics of groundwater in Mbanga, Njombe and Penja (Banana Plain)–Cameroon. J Afr Earth Sci 75:25–36

Allen DM, Suchy M (2001) Results of the groundwater geochemistry study on Saturna Island, British Columbia. Rapport final préparé pour: Islands Trust Victoria, B.C. Earths Sciences Simon Fraser University. 119p

Archie GE (1942) The electrical resistivity log as an aid in determining some reservoir characteristics. Trans Am Inst Min Metall Pet Eng 146:54–62

Atwia MG, Masoud AA (2013) Hydrochemical and geoelectrical investigation of the coastal shallow aquifers in El-Omayed area, Egypt. Environ Monit Assess 185(8):7065–7080

Banerjee P, Singh VS, Singh A, Prasad RK, Rangarajan R (2012) Hydrochemical analysis to evaluate the seawater ingress in a small coral island of India. Environ Monit Assess 184(6):3929–3942

Belkhiri L, Mouni L, Boudoukha A (2012) Geochemical evolution of groundwater in an alluvial aquifer: case of El Eulma aquifer, East Algeria. J Afr Earth Sci 66:46–55

Benkabbour B, Toto EA, Fakir Y (2004) Using DC resistivity method to characterize the geometry and the salinity of the Plioquaternary consolidated coastal aquifer of the Mamora plain, Morocco. Environ Geol 45:518–526

Bidet JC, Carruesco C (1982) Sedimentologie d'un environnement lagunaire actuel: l'Oulja de Oualidia (côte atlantique marocaine) Océanologica Aeta, n° SP, p. 29–37

Bugg SF, Lloyd JW (1976) A study of freshwater lense configuration in the Cayman Islands using resistivity methods. Q J Eng Geol 9:291–302

Cardona A, Carrillo-Rivera JJ, Huizar-Alvarez R, Graniel-Castro E (2004) Salinization in coastal aquifers of arid zones: an example from Santo Domingo, Baja California Sur, Mexico. Environ Geol 45:350–366

Cerling TE, Pederson BL, Von Damm KL (1989) Sodium–calcium ion exchange in the weathering of shales: implications for global weathering budgets. Geology 17(6):552–554

Chen K, Jiao JJ, Huang J, Huang R (2007) Multivariate statistical evaluation of trace elements in groundwater in a coastal area in Shenzhen, China. Environ Pollut 147:771–780

Choi BY, Yun ST, Kim KH, Kim JW, Kim HM, Koh YK (2014) Hydrogeochemical interpretation of South Korean groundwater monitoring data using self-organizing maps. J Geochem Explor 137:73–84

Choudhury K, Saha DK, Chakraborty P (2001) Geophysical study for saline water intrusion in a coastal alluvial terrain. J Geophys 46: 189–200

Davis JC (1986) Statistics and data analysis in geology. Wiley, New York, p 647

Dixon W, Chiswell B (1992) The use of hydrochemical sections to identify recharge areas and saline intrusions in alluvial aquifers, southeast Queensland. Aust J Hydrol 130:299–338

DRHT-FAO (1994) Elaboration d'un schéma d'exploitation des eaux souterraines du Sahel. Compte rendu final du projet FAO/TCP/MOR/2251

Duriez A, Marlin C, Dotsika E, Massault M, Noret A, Morel JL (2008) Geochemical evidence of seawater intrusion into a coastal geothermal field of central Greece: example of the Thermopylae system. Environ Geol 54(3):551–564

Dutta PS, Deb DL, Tyagi SK (1997) Assessment of ground water contamination from fertilizers in Delhi area based on 18O, NO3 and K composition. J Contam Hydrol 27:249–26

El Yaouti F, El Mandour A, Khattach D, Benavente J, Kaufmann O (2009) Salinization processes in the unconfined aquifer of Bou-Areg (NE Morocco): a geostatistical, geochemical, and tomographic study. Appl Geochem 24:16–31

Fadili A (2014) Etude hydrogéologique et géophysique de l'extension de l'intrusion marine dans le sahel de l'Oualidia (Maroc): analyse statistique, hydrochimie et prospection électrique. Thèse univ. Chouaïb Doukkali, Maroc. 289pp

Fakir Y, El Mernissi M, Kreuser T, Berjami B (2002) Natural tracer approach to characterize groundwater in the coastal Sahel of Oualidia (Morocco). Environ Geol 43:197–202

Farber E, Vengosh A, Gavrieli I, Marie A, Bullen TD, Mayer B, Holtzman R, Segal M, Shavit U (2004) The origin and mechanisms of salinization of the Lower Jordan River. Geochim Cosmochim Acta 68(9):1989–2006

Fehdi C, Rouabhia A, Baali F, Boudoukha A (2009) The hydrogeochemical characterization of Morsott-El Aouinet aquifer, northeastern Algeria. Environ Geol 58(7):1611–1620

Ferré M (1969) Hydrologie et hydrogéologie des Abda-Doukkala. Thèse de Docteur Ingénieur, Nancy. 407 p

Fetter CW (1993) Contaminant hydrogeology. Macmillan Pu- blishing Co., New York, 458p

Fidelibus MD, Tulipano L (1986) Mixing phenomena owing to sea water intrusion for the interpretation of chemical and isotopic data of discharge water in the apulian coastal carbonate aquifer (Southern Italy). Proceedings 9th Salt Water Intrusion Meeting, pp. 591–600

Fidelibus MD, Tulipano L (1996) Regional flow of intruding sea water in the carbonate aquifers of Apulia (Southern Italy). 14th Salt Water Intrusion Meeting. Rapporter och meddelanden nr 87, pp. 230–241

Fisher RS, Mullican WF (1997) Hydrochemical evolution of sodium–sulfate and sodium–chloride groundwater beneath the Northern Chihuahuan Desert, Trans-Pecos, Texas, USA. Hydrogeol J 10: 445–474

Frohlich RK, Urish DW, Fuller J, Reilley MO (1994) Use of geoelectrical method in groundwater pollution surveys in a coastal environment. J Appl Geophys 32:139–154

Giambastiani BMS, Colombani N, Mastrocicco M, Fidelibus MD (2013) Characterization of the lowland coastal aquifer of Comacchio (Ferrara, Italy): hydrology, hydrochemistry and evolution of the system. J Hydrol 501:35–44

Gigout M (1951) Etude géologique sur la meseta marocaine occidentale (arrière-pays de Casablanca, Mazagan et Safi). Notes et Mémoires du Service Géologique du Maroc, N°86, 2t, 507 pp

Gilli E, Mangan C, Mudry, J (2008) Hydrogéologie Objets, méthodes, applications Dunod, Paris

Grassi S, Cortecci G (2004) Hydrogeology and geochemistry of the multilayered confined aquifer of the Pisa plain (Tuscany - central Italy). Appl Geochem 20:41–54

Guerin R (2004) Contribution à l'hydrogéophysique. Habilitation à Diriger des Recherches, Univ. Paris IV, 262 p

Hamdan HA, Vafidis A (2013) Joint inversion of 2D resistivity and seismic travel time data to image saltwater intrusion over karstic areas. Environ Earth Sci 68(7):1877–1885

Han DM, Song XF, Currell MJ, Yang JL, Xiao GQ (2014) Chemical and isotopic constraints on evolution of groundwater salinization in the coastal plain aquifer of Laizhou Bay, China. J Hydrol 508:12–27

Hilali M (2002) Hydrogéologie et modélisation de l'intrusion marine dans les aquifères côtiers de Martil et du Sahel-Maroc. Thèse de Doctorat. Ecole Mohammadia d'Ingénieurs Rabat. 158p

Hodlur GK, Dhakate R, Sirisha T, Panaskar DB (2010) Resolution of freshwater and saline water aquifers by composite geophysical data analysis methods. Hydrol Sci J 55(3):414–434

Jones BF, Vengosh A, Rosenthal E, Yechieli Y (1999) Geochemical investigations. In: Seawater intrusion in coastal aquifers—concepts, methods and practices. Springer, Netherlands, pp 51–71

Kaid Rassou K, Fakir Y, Bahir M, Zouari K, Marah M (2005) Origine et datation des eaux souterraines du bassin hydrologique de la lagune d'oualidia. Estud Geol 61(3–6):191–196

Kass A, Gavrieli I, Yechieli Y, Vengosh A, Starinsky A (2005) The impact of freshwater and wastewater irrigation on the chemistry of shallow groundwater: a case study from the Israeli Coastal Aquifer. J Hydrol 300(1–4):314–331

Khairy H, Janardhana MR (2013) Hydrogeochemical features of groundwater of semi-confined coastal aquifer in Amol–Ghaemshahr plain, Mazandaran Province, Northern Iran. Environ Monit Assess 185(11):9237–9264

Kumar M, Ramanathan AL, Rao MS, Kumar B (2006) Identification and evaluation of hydrogeochemical processes in the groundwater environment of Delhi, India. Environ Geol 50:1025–1039

Loke MH, Barker RD (1996) Rapid least-squares inversion of apparent resistivity pseudosections by a quasi-Newton method. Geophys Prospect 44(1):131–152

Magaritz M, Nadler A, Koyumdjisky H, Dan N (1981) The use of Na/Cl ratio to trace solute sources in a semiarid zone. Water Resour Res 17: 602–608

Masoud AA (2014) Groundwater quality assessment of the shallow aquifers west of the Nile Delta (Egypt) using multivariate statistical and geostatistical techniques. J Afr Earth Sci 95:123–137

McCoy J (2004) ArcGIS 9: using ArcGIS Spatial Analyst. Esri Press

Meybeck M (1987) Global chemical weathering of surficial rocks estimated from river dissolved loads. Am J Sci 287(5):401–428

Morgan LK, Werner AD (2014) Seawater intrusion vulnerability indicators for freshwater lenses in strip islands. J Hydrol 508:322–327

Mtoni Y, Mjemah IC, Bakundukize C, Van Camp M, Martens K, Walraevens K (2013) Saltwater intrusion and nitrate pollution in the coastal aquifer of Dar es Salaam, Tanzania. Environ Earth Sci 70(3):1091–1111

Nadler A, Magaritz M, Mazor E (1980) Chemical reactions of seawater with rocks and freshwater: experimental and field observations on brackish waters in Israel. Geochim Cosmoch Acta 44:879–886

Naidu LS, VVS GR, Mahesh J, Padalu G, Sarma VS, Prasad PR, Rao SM (2013) An integrated approach to investigate saline water intrusion and to identify the salinity sources in the Central Godavari delta, Andhra Pradesh, India. Arab J Geosci 6(10):3709–3724

Nasher G, Al-Sayyaghi A, Al-Matary A (2013) Identification and evaluation of the hydrogeochemical processes of the lower part of Wadi Siham catchment area, Tihama plain, Yemen. Arab J Geosci 6(6): 2131–2146

Nowroozi AA, Stephen BH, Henderson P (1999) Saltwater intrusion into the freshwater aquifer in the eastern shore of Virginia: a reconnaissance electrical resistivity survey. J Appl Geophys 42:1–22

Ouadia M (1998) Les formations plio-quaternaires dans le domaine mésétien occidental entre Casablanca et Safi: Géomorphologie, Sédimentologie, Paléoenvironnements quaternaires et Evolution actuelle. Thèse d'Etat es Sciences. Univ. Mohammed V. Rabat, 319 p

Park SC, Yun ST, Chae GT, Yoo IY, Shin KS, Heo CH, Lee SH (2005) Regional hydrochemical study on salinization of coastal aquifers, western coastal area of South Korea. J Hydrol 313(3–4):182–194

Pascual M, Custodio E (1990) Geochemical observation in a continuously seawater intruded area: Garraf, Catalonia (Spain). Proc. 11th Salt Water Intrusion Meeting. Gdansk (Poland), 308–330

Rajesh R, Brindha K, Murugan R, Elango L (2012) Influence of hydrogeochemical processes on temporal changes in groundwater quality in a part of Nalgonda district, Andhra Pradesh, India. Environ Earth Sci 65(4):1203–1213

Rao NS, Rao PS (2009) Major ion chemistry of groundwater in a river basin: a study from India. Environ Earth Sci 61(4):757–775

Re V, Sacchi E, Martin-Bordes JL, Aureli A, El Hamouti N, Bouchnan R, Zuppi GM (2013) Processes affecting groundwater quality in arid zones: the case of the Bou-Areg coastal aquifer (North Morocco). Appl Geochem 34:181–198

Reddy AGS (2013) Evaluation of hydrogeochemical characteristics of phreatic alluvial aquifers in southeastern coastal belt of Prakasam district, South India. Environ Earth Sci 68(2):471–485

Rey J, Martínez J, Barberá GG, García-Aróstegui JL, García-Pintado J, Martínez-Vicente D (2013) Geophysical characterization of the complex dynamics of groundwater and seawater exchange in a highly stressed aquifer system linked to a coastal lagoon (SE Spain). Environ Earth Sci 70(5):2271–2282

Rogers RJ (1989) Geochemical comparison of groundwater in areas of New England, New York, and Pennsylvania. Groundwater 27(5): 690–712

Sami K (1992) Recharge mechanisms and geochemical processes in a semi-arid sedimentary basin, Eastern Cape, South Africa. J Hydrol 139:27–48

Schiavo MA, Hauser S, Cusimano G, Gatto L (2006) Geochemical characterization of groundwater and submarine discharge in the southeastern Sicily. Cont Shelf Res 26(7):826–834

Simler R (2004) Logiciel d'hydrochimie multilangage en distribution libre, Version 2. Laboratoire d'Hydrogéologie, Université d'Avignon, Avignon

Sonkamble S (2014) Electrical resistivity and hydrochemical indicators distinguishing chemical characteristics of subsurface pollution at Cuddalore coast, Tamil Nadu. J Geol Soc India 83(5):535–548

Srinivasamoorthy K, Gopinath M, Chidambaram S, Vasanthavigar M, Sarma VS (2014) Hydrochemical characterization and quality appraisal of groundwater from Pungar sub basin, Tamilnadu, India. J King Saud Univ-Sci 26(1):37–52

Stallard RF, Edmond JM (1987) Geochemistry of the Amazon 3.Weathering chemistry and limits to dissolved inputs. J Geophys Res 92:8293–8302

Stamatis G, Voudouris K (2003) Marine and human activity influences on the groundwater quality of southern Korinthos area (Greece). Hydrol Process 17:2327–2345

Tellam JH (1995) Hydrochemistry of the saline groundwaters of the lower Mersey Basin Permo-Triassic sandstone aquifer, UK. J Hydrol 165: 45–84

Tulipano L, Fidelibus MD (1984) Geochemical characteristics of Apulian coastal springs water (Southern Italy) related to mixing processes of ground waters with sea water having different residence time into the aquifer. Proceedings of the 5th international conference on water resources planning and management, Athens, 1–4 October, 2.55–2.67

Urish DW, Frohlich RK (1990) Surface electrical resistivity in coastal groundwater exploration. Geoexploration 26:267–289

Vandam JC, Meulankamp JJ (1967) Some results of the geo-electrical resistivity method in groundwater investigations in the Netherlands. Geophys Prospect 15:92–115

Vinson DS, Tagma T, Bouchaou L, Dwyer GS, Warner NR, Vengosh A (2013) Occurrence and mobilization of radium in fresh to saline coastal groundwater inferred from geochemical and isotopic tracers (Sr, S, O, H, Ra, Rn). Appl Geochem 38:161–175

Wanda E, Monjerezi M, Mwatseteza JF, Kazembe LN (2011) Hydrogeochemical appraisal of groundwater quality from weathered basement aquifers in Northern Malawi. Phys Chem Earth A/B/C 36(14): 1197–1207

Winter TC, Mallory SE, Allen TR, Rosenberry DO (2000) The use of principal component analysis for interpreting ground water hydrographs. Ground Water 32:234–246

Xing L, Guo H, Zhan Y (2013) Groundwater hydrochemical characteristics and processes along flow paths in the North China Plain. J Asian Earth Sci 70:250–264

Zohdy AAR (1969) The use of Schlumberger and equatorial soundings on groundwater investigations near El Psso Tx. Geophysics 34:713–728

Zouhri L (2010) Geoelectrical structure and hydrogeological investigations of the southern Rif Cordillera (Morocco). Hydrol Process 24: 1308–1317

Zouhri L, Carlier E, Ben Kabbour B, Toto EA, Gorini C (2008) Louche B, (2007) Groundwater interaction in the coastal environment: hydrochemical, electrical and seismic approaches. Bull Eng Geol Environ 67:123–128